Electrochimica Acta 56 (2011) 10083–10092

Contents lists available at SciVerse ScienceDirect

Electrochimica Acta

journal homepage: www.elsevier.com/locate/electacta

Influence of the substrate's surface structure on the mechanism and kinetics of the electrochemical UPD formation of a copper monolayer on gold

M. Palomar-Pardavé[a,*], E. Garfias-García[a], M. Romero-Romo[a], M.T. Ramírez-Silva[b], N. Batina[b]

[a] Universidad Autónoma Metropolitana-Azcapotzalco Departamento de Materiales, C.P. 02200, México, D.F., Mexico
[b] Universidad Autónoma Metropolitana-Iztapalapa, Departamento de Química, C.P. 09340, México, D.F., Mexico

ARTICLE INFO

Article history:
Received 26 July 2011
Received in revised form 26 August 2011
Accepted 28 August 2011
Available online 6 September 2011

Keywords:
Copper
Electrodeposition
UPD
Au(1 1 1)
Polycrystalline gold

ABSTRACT

The copper electrodeposition process was studied onto different gold substrates, single crystal (1 1 1) and polycrystalline, using electrochemical techniques. It was found, from the analysis of the experimental current density transients, that the potentiostatic formation of a full copper monolayer onto the gold electrode under UPD conditions follows the same mechanism, regardless of the crystallinity of the substrate. The mechanism involved the simultaneous presence of an adsorption process and of two 2D nucleation processes, progressive and instantaneous, respectively.

1. Introduction

In the last two and a half decades, the electrochemical scientific international community has devoted a great deal of attention to few fundamental aspects of the electrodeposition of metals [1], namely the mechanism and kinetics associated to the initial stages of formation of the first metallic nuclei. The main reason underlying such study preference, is that both aspects involve the significant occurrence of surface phenomena: for example, ordered adsorption, nucleation and growth, short-range phase transformations, cluster formation (including that of nanoparticles), and several others, which can be studied in depth. In view of the amount of information, particularly structural, that has been made increasingly available on the subject of underpotential deposition, UPD, it is only natural to expect the publication of authoritative works correlating the aforementioned with other aspects of UPD phenomena of the first metal monolayer, over a foreign substrate [2–9]. Consequently, such efforts have contributed to a significant increase of the fundamental understanding of electrochemical phase formation. However, the influence of the substrate's structure on the mechanism and kinetics of the monolayer formation, which entails formation of a new 2D phase growing on the surface of the substrate, has been relatively less studied [9]. The structure of the substrate surface plays an important role in its own right, as it determines specific features of the growing deposit, particularly during the first stages of the deposition process. The polycrystalline metal electrodes [10–15] do display a complex crystallographic character, bearing quite a large variety of surface orientations, separated by a network of grain boundaries, also with other emerging structural faults inherited from the mechano-thermal history of the substrate. Thus, diverse studies have attempted to relate the formation of monolayers onto such surfaces, being rather limited, insofar as the mechanism and the kinetics of formation concerned. The conventional electrochemical methods generally involve one macroscopic measurement, namely that of the current passing through the system, which makes it sufficiently difficult to differentiate among the diverse contributions to the overall current, likely to arise in association with those of the crystallographic variety. This is, the grain boundaries and other defects of the polycrystalline system must be considered an inherent part of the working electrode, because they may influence the measurement of relevant parameters like the density number of nucleating sites. The utilization of single crystal electrodes has helped us to study in a more systematic manner the influence of the surface morphology of the substrate upon the electrocrystallization process [2–9]. The formal study of interfacial phenomena is particularly well suited when basic data emerges from the analysis of the temporal response of the current passing through an electrode which is under potentiostatic control [16–32]. For this matter, the framework of several theoretical formalisms associated with metal electrodeposition, allow discernment of the dimensionality of the deposit, the rate limiting step for

* Corresponding author.
E-mail addresses: mepp@correo.azc.uam.mx, mpalomar@hotmail.com (M. Palomar-Pardavé).

0013-4686/$ – see front matter © 2011 Elsevier Ltd. All rights reserved.
doi:10.1016/j.electacta.2011.08.105

the overall process, as well as the determination of a reduced variety of kinetic parameters that have physical meaning. In view of the aforementioned, this research work deals with the application of chronoamperometry to study the initial stages of the formation and growth of copper nuclei onto gold electrodes like, Au(1 1 1), and Au polycrystalline from an aqueous 1 mM $CuSO_4$ solution in 1 M H_2SO_4.

2. Experimental

All experiments were performed within a typical three-electrode electrochemical cell, where a nitrogen atmosphere was circulated over the electrolyte to prevent oxygen dissolution. The working electrode was a 200 nm gold layer, supported on a heat-resistant glass substrate (Berlin Glass). The surface of the vacuum-deposited gold layer is (1 1 1), and could be safely annealed under a hydrogen flame. Other experiments were performed with a BAS polycrystalline gold tip of a rotating disc electrode, having 0.0707 cm^2 exposed working area. Cyclic voltammograms were obtained at pH 1 under UPD conditions, with the potential scans starting at 0.8 V vs. Cu^{2+}/Cu toward the negative direction at 15 mV s^{-1} scan rate. The gold electrode surface area was observed with a Scanning Tunneling Microscope, Digital Instruments NanoScope IIIa, in the case of the single crystal Au(1 1 1) and for the polycrystalline electrode an Olympus PMG3 metallographic microscope was used.

3. Results and discussion

3.1. Theoretical considerations

When a metal (Me) is in contact with a solution containing its ions (Me^{z+}), it can adopt its equilibrium potential E_{eq} generally referred to as the reversible Nernst potential given by the following equation:

$$Me^{z+}_{sol} + ze^- \underset{b}{\overset{a}{\rightleftarrows}} Me \tag{1}$$

which is described through the well known Nernst equation below

$$E_{eq} = E^0 + \frac{RT}{zF}\ \ln\frac{(Me^{z+}_{sol})}{(Me)} \tag{2}$$

where z is the electron's number, F is Faraday's constant and E^0 is the standard potential for reaction (2) and E^0 gives the metal ions' activity. However, in concentration terms of the species involved, E_{eq} is described by Eq. (3):

$$E_{eq} = E^0 + \frac{RT}{zF}\ \ln\frac{\gamma_{Me^{z+}_{sol}}[Me^{z+}_{sol}]}{\gamma_{Me}[Me]} \tag{3}$$

As it is somewhat inconvenient to deal numerically with activities, because the activity coefficients are mostly unknown, thus it is customary to use the potential known as formal potential $E^{0'}$, which brings in the standard potential and some of activity coefficients, such that:

$$E^{0'} = E^0 + \frac{RT}{zF}\ \ln\frac{\gamma_{Me^{z+}_{sol}}}{\gamma_{Me}} \tag{4}$$

Then, the definition of $E^{0'}$ using also Eq. (2), can be written as:

$$E_{eq} = E^{0'} + \frac{RT}{zF}\ \ln\frac{[Me^{z+}_{sol}]}{[Me]} \tag{5}$$

Eq. (5) allows relating E_{eq} to the concentrations of the species involved. However, as the ionic strength influences the activity, the $E^{0'}$ for the same reaction will vary from one medium to the next, even in the case when, due to change in the study medium, there were no stable complexes formed between the metal ions and any of the components of the new medium, Y^{j-}_{sol}. For the case when different species of the metal ions are formed, $[Me(Y)_i]^{z-(i\times j)}_{sol}$, then $E^{0'}$ will also comprise terms involving the equilibrium constants and concentrations of some of the species involved during the complexation equilibrium. This is, particularly, the case of complexation reaction (6), where the metal ion Me^{z+} is involved, as follows:

$$Me^{z+}_{sol} + iY^{j-}_{sol} \underset{b}{\overset{a}{\rightleftarrows}} [Me(Y)_i]^{z-(i\times j)}_{sol} \tag{6}$$

with an equilibrium constant given as:

$$K(T) = \frac{[[Me(Y)_i]^{z-(i\times j)}_{sol}]]}{[Me^{z+}_{sol}] \times [Y^{j-}_{sol}]^i} \tag{7}$$

Then, E_{eq} must be estimated to produce Eq. (8) instead of Eq. (1):

$$[Me(Y)_i]^{z-(i\times j)}_{sol} + ze^- \underset{b}{\overset{a}{\rightleftarrows}} Me + iY^{j-}_{sol} \tag{8}$$

This is done using (4), (5) and (7), which gives (9)

$$E_{eq} = E^0 + \frac{RT}{zF}\ \ln\frac{\gamma_{Me^{z+}_{sol}}}{\gamma_{Me}} + \frac{RT}{zF}\ \ln\frac{[[Me(Y)_i]^{z-(i\times j)}_{sol}]}{[Me] \times K(T) \times [Y^{j-}_{sol}]^i} \tag{9}$$

Now, defining $E^{0'}$ as (10), as follows:

$$E^{0'} = E^0 + \frac{RT}{zF}\ \ln\frac{\gamma_{Me^{z+}_{sol}}}{\gamma_{Me}} - \frac{RT}{zF}\ \ln K(T) - i\frac{RT}{zF}\ \ln[Y^{j-}_{sol}] \tag{10}$$

The corresponding Nernst equation is now obtained:

$$E^0 = E^{0'} + \frac{RT}{zF}\ \ln\frac{[[Me(Y)_i]^{z-(i\times j)}_{sol}]}{Me} \tag{11}$$

It follows from the treatment above, that quantitative thermodynamic data on E_{eq} of the solution studied is necessary.

The application of an electrode potential (E) more positive than E_{eq}, brings about the dissolution of the metal (refer to direction b in Eq. (1)), while for a potential more negative than the E_{eq} ($E < E_{eq}$), the metal ions will be reduced over the surface of the electrode, until a new equilibrium is reached. However, when a metal is deposited on a different metallic substrate, namely Cu on Au, rather than Cu on Cu, an apparent violation of the Nernst's Law becomes evident: the first monolayer is deposited at potentials more positive than the respective Nernst potential (E_{eq}). Such behavior has been termed underpotential deposition, UPD, which contrasts with the deposition processes taking place at overpotential, OPD. However, it must be remembered that in spite of the symmetry of the technical terms UPD and OPD, the physical origin of both effects is quite different. It becomes apparent that the reason for the OPD is only due to the kinetics of the deposition process, while that of the UPD is related to the energetics of the adatom-substrate bond.

The UPD deposit of metals has been extensively described in an authoritative revision [1,2]. The effect of the deposit at underpotential conditions is more conveniently demonstrated with cyclic voltammetry experiments, where the current observed is due to the electrochemical reaction taking place as the potential is continuously changed, with dE/dt constant within a selected range. The formation (dissolution) of the first monolayer is easily detected because pronounced current peaks at $E \geq E_{eq}$ become clearly apparent during the cathodic (anodic) potential scan, whereas the massive deposit (overpotential deposition, opd) or multilayeres takes place only when $E < E_{eq}$. The fact that the first layer forms at much more positive potentials than those necessary for the massive deposit, simply means that the metal ad-atoms develop a stronger

Table 1
Theoretical determination of the equilibrium potential E_{eq} for the pair Cu(II)/Cu(0) in a 1.0 mM Cu(II), 0.1M H_2SO_4 aqueous dissolution at different pH.

pH	I/mol L^{-1}	Cu(II)′	Theory	$\gamma_{Cu(II)'}$	E_{eq}/mV vs. Cu^{2+}/Cu
1.0	0.1	$Cu(H_2O)_6^{2+}$	DHE[a]	0.32	35
			DHL[b]	0.22	30
			D[c]	0.37	37
4.0	0.3	$CuSO_4$	DHE	0.19	−13
			DHL	0.07	−25
			D	0.29	−8

[a] Debye-Hückel extended.
[b] Debye-Hückel limit.
[c] Davies.

interaction, basically dependent on the energetics of this particular system, with the nearby substrate of a different nature than their own, on which they will be bonded, than to a substrate of its own type.

At the copper concentration considered in this work (1.0 mM) the predominating species were the $Cu(H_2O)_6^{2+}$ ion at pH 1 and the soluble $CuSO_4$ complex at pH 4. It is worth noting also that the SO_4^{2-} species will depend on the solution pH, with the bisulphate anion (HSO_4^-) at pH 1 and the (SO_4^{2-}) at pH 4. Considering this, the ionic strength of the solution changes with pH, from 0.1 at pH 1 to 0.3 at pH 4.

Table 1 gives the values for E_{eq} that were theoretically estimated using Eq. (3), as a function of the ionic strength (I) of the medium, where the activity coefficients were calculated by means of the extended and limited Debye-Hückel theories, and also by the Davies theory of the approach used to estimate the value of the activity coefficient for the Cu(II) ion ($\gamma_{Cu(II)'}$) for the generalized reaction (12):

$$Cu(II)' + 2e^- \underset{b}{\overset{a}{\rightleftharpoons}} Cu(0) \qquad (12)$$

As can be noted, in the reaction Cu(II)′ represents the predominating copper species which is present, according to the chemical features of the medium considered, namely pH and pSO_4.

3.2. Cyclic voltammetry

The results shown in Fig. 1 correspond to the cyclic voltammetry study performed in the system: 1.0 mM Cu(II), 0.1 M H_2SO_4 at pH 1.0, with two different gold electrodes: Au (1 1 1) single crystal and polycrystalline Au. For both cases, it can be observed that copper deposition has taken place at potentials more positive than the equilibrium potential for the $Cu(H_2O)_6^{2+}$/Cu(0) pair; therefore, this deposit corresponds to copper UPD onto gold. In the particular case of the Au(1 1 1) single crystal, the formation of two voltammetric peaks, namely A and B, can be distinguished when the potential was scanned toward more negative values. It is important to remark that this voltammogram possesses the same features than those reported by Hölzle et al. [3] and Wieckowski et al. [33,34], in the same system. The peaks indicate the presence of at least two processes energetically different, which are responsible for the copper underpotential electrodeposition onto the Au(1 1 1). However, when deposition took place onto the polycrystalline electrode, the first peak (Fig. 1, peak A) appeared frankly inhibited. Instead of two peaks A and B, there only appears one peak E. Peaks C and D and peak F correspond to the oxidation of the copper adlayer previously electrodeposited onto Au(1 1 1) and polycrystalline, respectively.

From Fig. 1 it is possible to see that reversing the potential scan toward more positive values, two peaks C and D become noticeable for the single crystal electrode, while just one peak F appeared for the polycrystalline. These peaks are associated with the dissolution of the copper deposited during the direct scan. From the

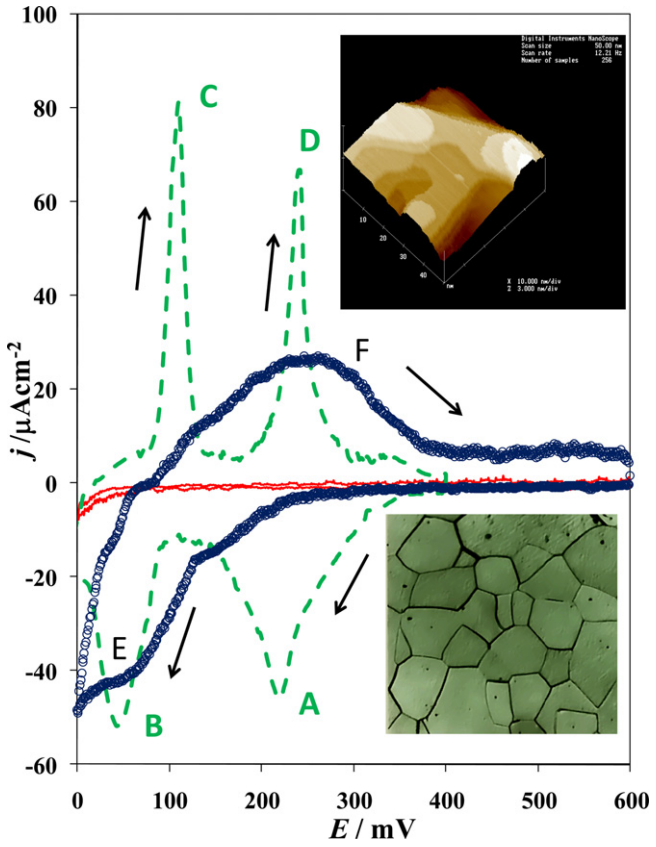

Fig. 1. Typical cyclic voltammograms obtained for the system Au/1 mM $CuSO_4$, 0.1 M H_2SO_4 with two different electrodes: single crystal (green) and polycrystalline (blue). The trace running almost flatly parallel to zero current (red) corresponds to the response obtained in the same system in the absence of the Cu(II) ions (blank). In all cases, the potential scan started at 800 mV vs. Cu^{2+}/Cu in the negative direction, as indicated by the arrows, at 15 mV s^{-1} potential scan rate. Insets show the STM, 40 nm × 40 nm × 10 nm, (up) and micrographic, 70×, (down) images corresponding to the electrode surface of the Au (1 1 1) and polycrystalline gold, respectively. (For interpretation of the references to color in this figure legend, the reader is referred to the web version of the article.)

literature, the copper deposited under UPD conditions onto the Au(1 1 1) has been characterized by means of sophisticated surface techniques such as LEED (low energy electron diffraction), RHEED (reflection high energy electron diffraction), EELS (electron energy loss spectroscopy) and XRD (X-ray diffraction), among others. As a result, Kolb showed [2] the structural changes that the UPD copper deposit undergoes on Au(1 1 1). Fig. 2 shows the potential variation as a function of the degree of coverage with copper atoms on the Au(1 1 1) electrode, and the scheme of the structure attained by the deposit. It can be observed that for a lower degree of coverage, at a potential more positive than for peak A of the cyclic voltammetry plot referred above, the adsorption of copper atoms seems random; for intermediate coverage, that is at a potential between peaks A and B, the adsorption observed appeared ordered adopting a structure $\left(\sqrt{3} \times \sqrt{3}\right)$ R30° (honeycomb shape). Lastly, for more negative potentials as compared to peak B, a (1 × 1) structure describes the complete monolayer (ML) formed. It is also important to mention that Wieckowski et al. [33,34], from a computational and theoretical lattice-gas modeling approach and electrochemical and UHV experiments, contributed to clarify the situation about the structure of copper UPD on Au(1 1 1). They found that in the potential region between the two sharp CV peaks, the electrode is covered by a mixed adlayer of $\left(\sqrt{3} \times \sqrt{3}\right)$ R30° symmetry, consisting of 2/3 ML Cu and 1/3 ML sulfate. This ordered-phase region is limited on the positive-potential side by a first-order phase transition to a

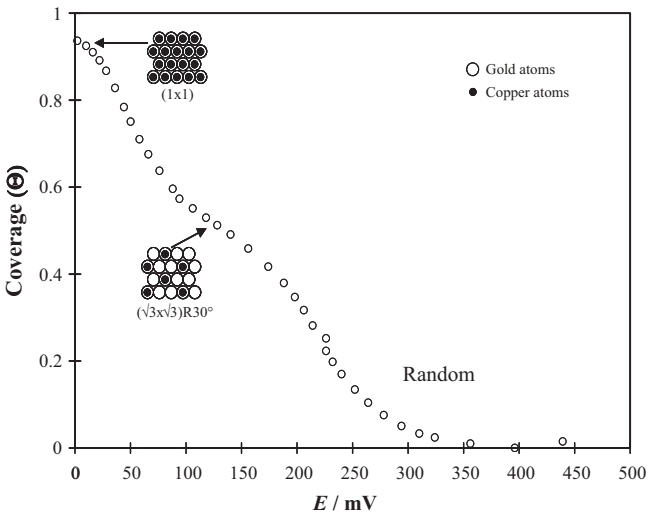

Fig. 2. Variation of the coverage degree (Θ) of copper atoms onto Au(1 1 1) as a function of the applied potential under UPD conditions, from a 1.0 mM $CuSO_4$, 0.1 M H_2SO_4 aqueous solution at pH 1.0. The structural schemes refer to the structures adopted by the copper layer deposited, as determined by LEED and RHEED from Kolb's work [2].

disordered low-coverage phase, followed at still higher potentials by transitions to pure sulfate phases. On the negative-potential side the mixed phase terminates at a second-order phase transition to a full monolayer of Cu. Moreover, they pointed out the necessity to investigate the kinetics of the deposit's formation.

Fig. 3 shows the charge density variation (q) as a function of the potential applied to the electrode during the voltammetry copper deposition process at underpotential conditions onto the two kinds of gold electrodes, single crystal and polycrystal, as obtained by integrating the cathodic branch of the corresponding voltammograms presented in Fig. 1. In spite of the different forms in which q varies with E for each of the electrodes, it is important to note that upon applying a potential near the equilibrium potential, namely *ca.* 0 V vs. Cu^{2+}/Cu, a q value nearing 420 $\mu C\,cm^{-2}$ was obtained for both types of electrodes. This value falls quite near the theoretical value corresponding to the formation of a copper isomorphous layer on gold, which is 440 $\mu C\,cm^{-2}$, corresponding to a copper monolayer. Clearly, the result indicates that at values near the equilibrium potential whether on a gold single crystal or polycrystal, a copper monolayer is formed, even though its formation kinetics (see the graph trajectory) may be different, depending on the crystallinity of the substrate.

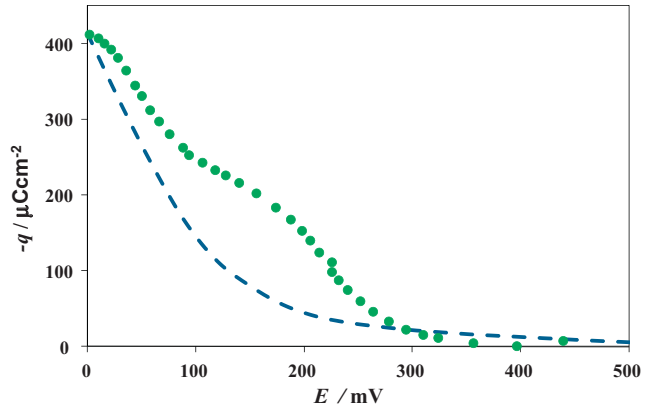

Fig. 3. Charge density variation as a function of the applied potential during the copper UPD, from a 1 mM $CuSO_4$, 0.1 M H_2SO_4 aqueous solution, onto two types of gold electrodes: single crystal Au(1 1 1) (green dots) and polycrystalline gold (blue broken line). (For interpretation of the references to color in this figure legend, the reader is referred to the web version of the article.)

3.3. Potentiostatic current transients

It should be stated that as a background to the studies undertaken in this part of the work, Hölzle et al. [3], studied the copper underpotential deposition onto Au(1 1 1) using potentiostatic current transients. Their relevant contribution concerns the mechanism proposed that described the experimental potentiostatic current transients, involving the simultaneous presence of the double layer charge transfer process involving a Langmuir-type adsorption–desorption equilibrium [3,24,26] (refer to Eq. (13)), and a 2D instantaneous nucleation process (refer to Eq. (14)).

$$j_{ad} = K_1 \exp(-K_2 t) \tag{13}$$

where t is the perturbation time, $K_1 = E/R_s$, $K_2 = 1/R_s C$

$$j_{2Di-LI}(t) = P_1 t \exp(-P_2 t^2) \tag{14}$$

with $P_1 = 2\pi z F M h N_0 K_g^2/\rho$ and $P_2 = \pi M^2 N_0 K_g^2/\rho^2$

For all the equations, unless otherwise stated, E represents the applied potential throughout the perturbations, R_s is the solution's resistance, C the double layer capacitance, K_g represents the nuclei growth rate constant (mol $cm^{-2}\,s^{-1}$), M and ρ are the molecular mass and the density of the deposit, respectively, h is the height of the layer formed and N_0 is the overall number density of active sites available for the nucleation process on the surface of the substrate.

This model was particularly adequate to describe the copper underpotential deposition process onto a Au(1 1 1) substrate [3], when the potential pulse (E_{ar}) initiated at an intermediate potential value ≅100 mV vs. Cu^{2+}/Cu between peaks A and B, see Fig. 1 and finished at various other different potentials (E), around the equilibrium potential. It should be noted though, that under the conditions stated by Hölzle et al. [3], the potentiostatic pulse studies do begin with a Au(1 1 1) surface which already has approximately 70% of the atomic coverage required to form a copper monolayer, as can be appreciated from Fig. 2.

However, when Hölzle et al. [3], studied the copper deposition under peak A, starting the potential pulse at a value E_{ar} = 400 mV, where the Au(1 1 1) surface was copper-free (see Figs. 2 and 3), and finishing at different potential values belonging to peak A, so that approximately a half of the monolayer would have been effectively deposited, it was found that the shape of the transient obtained did not show evidence of a nucleation process. It means they did not studied the full formation of the monolayer, starting out with a copper-free Au(1 1 1) surface. Contrary, here in our work we investigate full formation of the copper monolayer (UPD) starting from a copper-free Au(1 1 1) surface, for which the following results will attempt to reveal new insights on the fundamentals of this process. It is relevant to mention that attempts to describe electrochemical phase formation processes have been made using Kinetic Monte Carlo simulations of current transients, see for instance the work of Scharifker et al. [18], for silver and mercury electrodeposition onto a vitreous carbon electrode and that of Brown et al. [35], for copper UPD on Au(1 1 1) in sulfate media. In particular Brown et al. [35], using numerical (dynamic Monte Carlo simulations) studies of lattice-gas models that treat copper and sulfate as interacting particles that compete for the same adsorption sites where the energy barriers were assumed to vary according to the Butler-Volmer approximation, found a very good agreement between their simulations and the experiments of Hölzle et al. [3], in both positive-going and negative-going steps. Notwithstanding, neither Hölzle et al. [3], nor Brown et al. [35], considered for their respective studies, the full formation of the copper monolayer (UPD) starting from a copper-free Au(1 1 1) surface in a single potential step experiment.

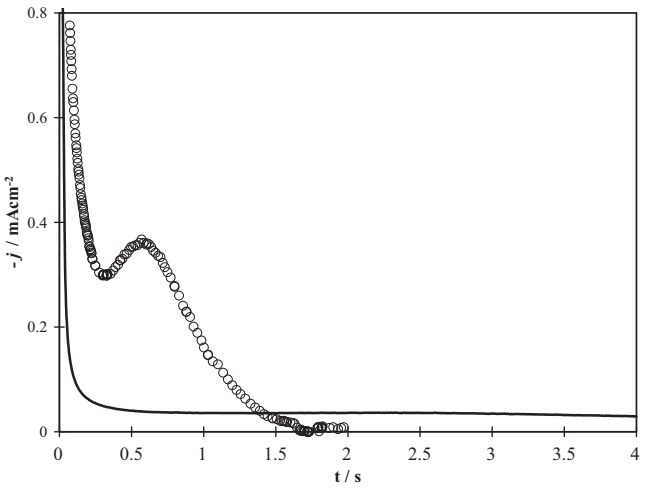

Fig. 4. Typical potentiostatic current transients obtained during copper underpotential deposition onto Au(1 1 1) (circles) and polycrystalline gold (line) from a 1.0 mM $CuSO_4$ in 0.1 M H_2SO_4 aqueous solution at pH 1.0. The potential step started at E_{ar} = 600 mV and ended at 5 mV in both cases.

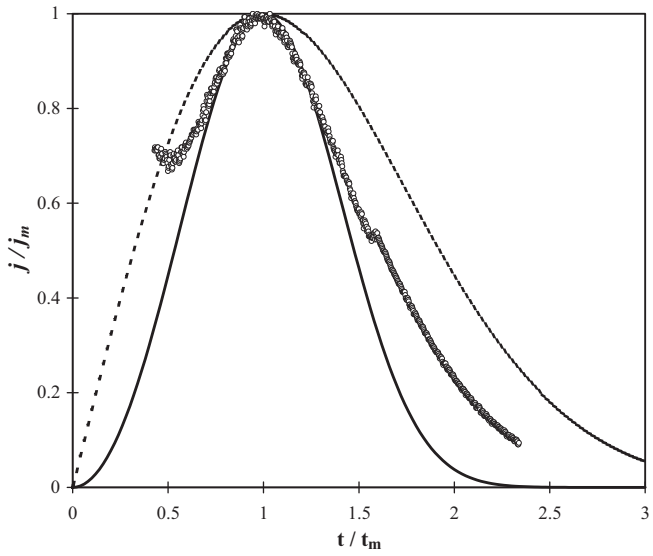

Fig. 5. Comparison between the predicted theoretical plots for a 2D nucleation process limited by the incorporation of ad-atoms: instantaneous (broken line) and progressive (solid line) and the experimental transient (circles) shown in Fig. 4 for the Au(1 1 1) electrode, normalized through their respective co-ordinates for the current maximum.

Fig. 4 shows two potentiostatic current transients obtained during copper UPD onto Au(1 1 1) and onto the polycrystal surface, both free from copper ad-atoms (E_{ar} = 600 mV). The values of the applied potentials (E) correspond to values close to the equilibrium potential. In both cases the overall charge density involved, calculated by integrating the $-j$ vs. t plot, appeared very close to the theoretical value found for a Cu pseudomorphic monolayer (1×1) on Au(1 1 1) [22].

3.3.1. Electrochemical formation of the copper monolayer on Au(1 1 1)

The shape of the potentiostatic current transients for times longer than 0.4 s appeared similar to that predicted for the nucleation and growth of 2D centres limited by the incorporation of ad-atoms. The maximum indicates that the centres have grown to an extent that coalescence prevailed. For times shorter than 0.4 s, the transients displayed a shape which could not be described by any of the nucleation models, unless the contribution of an adsorption process is taken into consideration in the expression for the overall current density (see Eq. (13)). Therefore, the shape of the transients obtained can apparently be explained by the process described by Hölzle et al. [3], whereby the overall current density (j) comprises the linear addition of an adsorption process (j_{ad}) plus a 2D nucleation ($j_{2D\text{-}LI}$) process limited by the incorporation of ad-atoms, as indicated in Eq. (15).

$$j = j_{ad} + j_{2D-LI} \tag{15}$$

where j_{ad} is described by Eq. (13) and $j_{2D\text{-}LI}$ by Eq. (14) for instantaneous or (16) for progressive nucleation mechanism [1,24–26].

$$j_{2Dp-LI}(t) = P_3 t^2 \exp(-P_4 t^3) \tag{16}$$

where $P_3 = \pi z F M h A N_0 K_g^2/\rho$ and $P_4 = \pi M^2 A N_0 K_g^2/3\rho^2$

In these equations, A represents the nucleation rate constant.

To discern which of Eq. (14) or (16) represent best the 2D nucleation process, it becomes necessary to classify the experimental nucleation mechanism; in order to do this we followed the method described elsewhere [25].

Fig. 5 shows a comparison of a selected region of the transients corresponding to the Au(1 1 1) electrode, shown in Fig. 4, which have been normalised through the co-ordinates of their respective maximum, with the theoretical dimensionless plots that are associated to instantaneous and progressive nucleation [3]. Generally speaking, it can be observed to begin with, that the results for the experimental nucleation support that, when $t/t_m \leq 1.5$, this follows relatively closely the progressive nucleation; while for values greater than those given by the relation, the experimental nucleation appears located between the instantaneous and progressive mechanisms.

The comparison shown in Fig. 5, suggests that in this case the nucleation cannot be easily classified as instantaneous or progressive within the whole time period considered, this being in principle a problem that requires to be solved. Hence, as the doubt persists: which of Eq. (14) or (16), instantaneous or progressive, respectively, would be more convenient to use in Eq. (15) to represent the 2D nucleation process? Therefore, non-linear fitting of Eq. (15) was performed to the experimental transients, and each of the two possibilities considered separately. First, if the instantaneous mechanism is considered for the 2D nucleation, Eq. (15) becomes Eq. (17) as follows:

$$j = j_{ad} + j_{2Di-LI} \tag{17}$$

where the $j_{2Di\text{-}LI}$ is represented by means of Eq. (14). Fig. 6 shows the comparison between the experimental transient obtained using the Au(1 1 1) electrode, see Fig. 4, and the transient obtained by means of non-linear fitting of Eq. (17) to the experimental data. The result of the fitting is considered satisfactory for the initial part of the experimental transient. However, the description of the data points from about t = 0.35 s up to the maximum is rather poor.

Trying now the 2D progressive nucleation mechanism, Eq. (15) now becomes Eq. (18):

$$j = j_{ad} + j_{2Dp-LI} \tag{18}$$

where the contribution due to $j_{2Dp\text{-}LI}$ is represented by Eq. (16).

Fig. 7 shows the results obtained using the aforementioned mechanistic considerations; now the description of the overall transient is still less precise than the previous one, except of course, for the initial part, which would appears to be well fitted.

In view of the comparative results concerning the experimental potentiostatic current transients, see Figs. 6 and 7, and the dimensionless plots for the instantaneous and progressive nucleation, Fig. 5, it would appear to be feasible that the following mechanism, depicted by Eq. (19), should describe appropriately the underpotential deposition of copper onto Au(1 1 1) involving complete

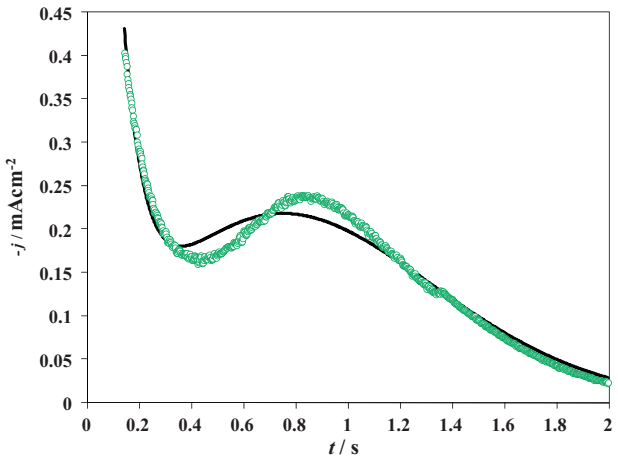

Fig. 6. Comparison between the experimental potentiostatic current transient (green circles) obtained during formation of a copper monolayer onto Au(1 1 1), under the conditions stated in Fig. 4, and a theoretical transient (line) obtained through non-linear fitting of Eq. (17) to the experimental data. (For interpretation of the references to color in this figure legend, the reader is referred to the web version of the article.)

formation of a monolayer of the metal, where the surface was initially free from copper ad-atoms.

$$j = j_{ad} + j_{2Dp-LI} + j_{2Di-LI} \quad (19)$$

Eq. (19) brings about the possibility to deconvolute the overall current of the experimental transients into three individual contributions corresponding to three different processes, which take place during the copper UPD onto Au(1 1 1) under the conditions stated before; namely, an adsorption process and two nucleation processes. Fig. 8 presents a comparison of the non-linear fitting of Eq. (19) to the experimental transient. It becomes noticeable that the fitting process is indeed adequate to describe the overall current transient. The figure also shows the plots of the individual contributions to the overall current, noting that the nucleation processes are fully overlapping and that the overall current at the end of the transient is mainly due to the 2Di-Ll nucleation process.

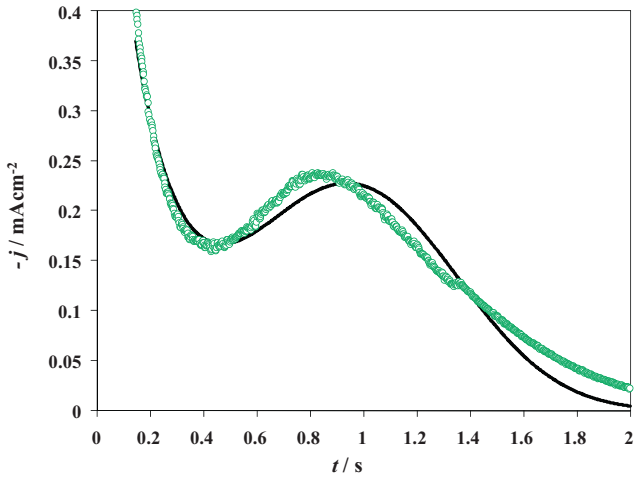

Fig. 7. Comparison between the experimental potentiostatic current transient (green circles) obtained during formation of a copper monolayer onto Au(1 1 1), under the conditions stated in Fig. 4, and a theoretical transient (line) obtained through non-linear fitting of Eq. (18) to the experimental data. (For interpretation of the references to color in this figure legend, the reader is referred to the web version of the article.)

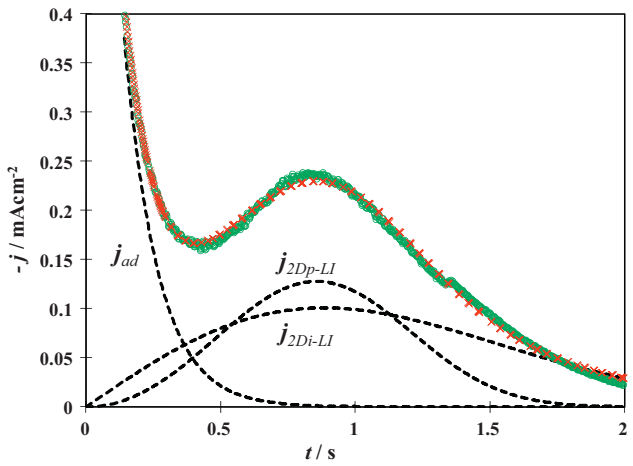

Fig. 8. Comparison between the experimental potentiostatic current transient (green) obtained during formation of a copper monolayer onto Au(1 1 1), under the conditions stated in Fig. 4, and a theoretical transient (red) obtained through non-linear fitting of Eq. (19) to the experimental data. The individual contributions to the overall current have also been plotted that are due to an adsorption process (j_{ad}), a progressive 2D nucleation process limited by ad-atom incorporation (j_{2Dp-LI}) and an instantaneous 2D nucleation process, limited also by incorporation of ad-atoms (j_{2Di-LI}). (For interpretation of the references to color in this figure legend, the reader is referred to the web version of the article.)

3.3.2. *Influence of the applied potential on Cu UPD onto Au(1 1 1)*

Fig. 9 shows a family of potentiostatic current transients obtained during copper UPD deposition on a copper *ad-atoms*-free Au(1 1 1) surface at (E_{ar} = 600 mV). The values of the applied potential pulses (E) correspond to the more negative potential zone of the voltammogram shown in Fig. 1.

Fig. 10 shows the results from the fitting procedure of all the other transients through Eq. (19). It can be observed that as the applied potential becomes more cathodic the instantaneous nucleation becomes more important, whereas the opposite is true with the progressive nucleation. The best fitting parameters are shown in Table 2, which includes K_1 and K_2 that correspond to the adsorption process (refer to Eq. (13)), parameters P_1 and P_2 belong to the 2D instantaneous nucleation process (refer to Eq. (14)) and the parameters P_3 and P_4 are associated to 2D progressive nucleation process (refer to Eq. (16)).

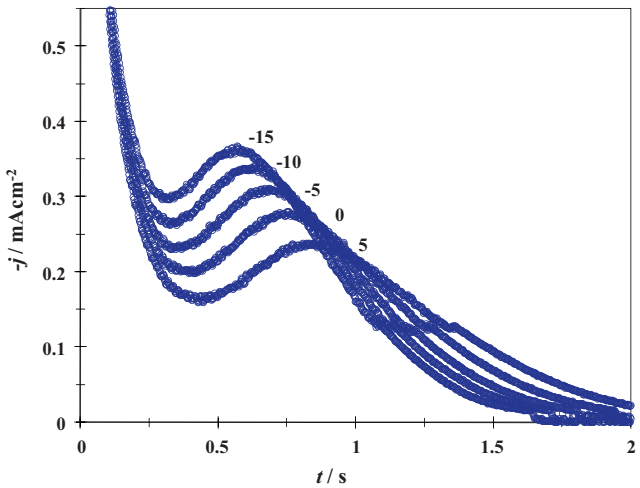

Fig. 9. Family of potentiostatic current transients obtained during copper UPD on a copper *ad-atoms*-free Au(1 1 1) surface from a 1.0 mM $CuSO_4$, 0.1 M H_2SO_4 aqueous solution at pH 1.0. The applied potentials, mV, are duly indicated in the figure. The E_{ar} was for all cases 600 mV.

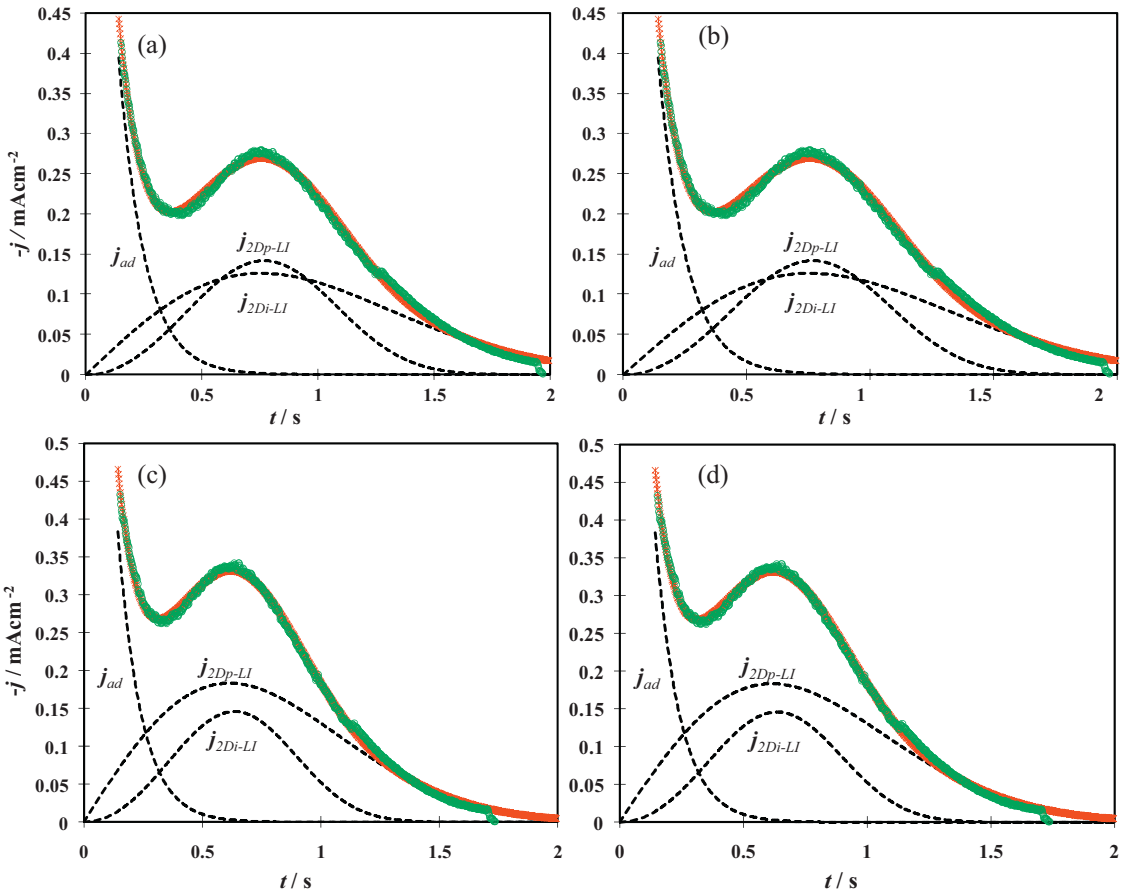

Fig. 10. Comparison between the experimental potentiostatic current transients (green) obtained with (a) 0 mV, (b) −5 mV, (c) −10 mV and (d) −15 mV, under the conditions stated in Fig. 9 and their respective theoretical transients (red) obtained through non-linear fitting of Eq. (19) to the experimental data. The individual contributions to the overall current have also been plotted that are due to an adsorption process (j_{ad}), a progressive 2D nucleation process limited by ad-atom incorporation ($j_{2Dp\text{-}LI}$) and an instantaneous 2D nucleation process, limited also by incorporation of ad-atoms ($j_{2Di\text{-}LI}$). (For interpretation of the references to color in this figure legend, the reader is referred to the web version of the article.)

Table 2
Current maxima coordinates and best fitting parameters obtained through non-linear fitting of Eq. (19) to the experimental transients shown in Fig. 10.

E/mV	t_m/s	j_m/mA cm^{-2}	K_1/mA cm^{-2}	K_2/s^{-1}	10^4P_1/C cm^{-2} s^{-3}	P_2/s^{-3}	10^4P_3/C cm^{-2} s^{-3}	P_4/s^{-3}
−15	0.57	0.367	1.85	10.93	6.77	1.61	6.84	3.15
−10	0.63	0.339	1.61	10.04	4.93	1.33	6.70	2.59
−5	0.68	0.310	1.47	9.32	3.46	1.07	6.34	2.0
0	0.76	0.279	1.40	8.89	2.74	0.88	4.69	1.48
5	0.85	0.238	1.18	8.00	1.88	0.64	3.4	1.06

The K_2 potential dependence can be, in agreement with Noël and Vasu [36] modeled by means of a Butler–Volmer-type expression. The adsorption of metal ions associated to the charge transfer is described by the following expression (20):

$$K_2 = K_a^0 \ \exp\left(-(1-\beta)\frac{zFE}{RT}\right) \tag{20}$$

Taking logarithms on each member of (20) the following relation is obtained (21)

$$\log\ K_2 = \log\ K_a^0 - \frac{(1-\beta)zF}{2.303RT}E \tag{21}$$

Eq. (21) indicates that the log(K_2) variation with the applied potential ($-E$), should give a straight line with slope (m) equal to (22)

$$m = \frac{\partial \log\ K_2}{\partial(-E)} = \frac{(1-\beta)zF}{2.303RT} \tag{22}$$

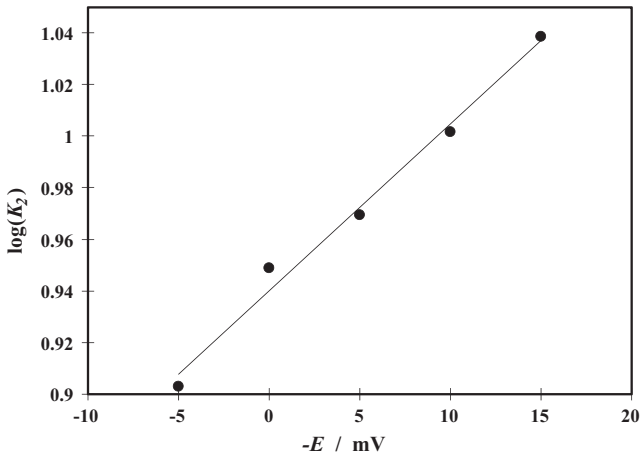

Fig. 11. Potential variation of K_2. The line corresponds to the data's linear regression.

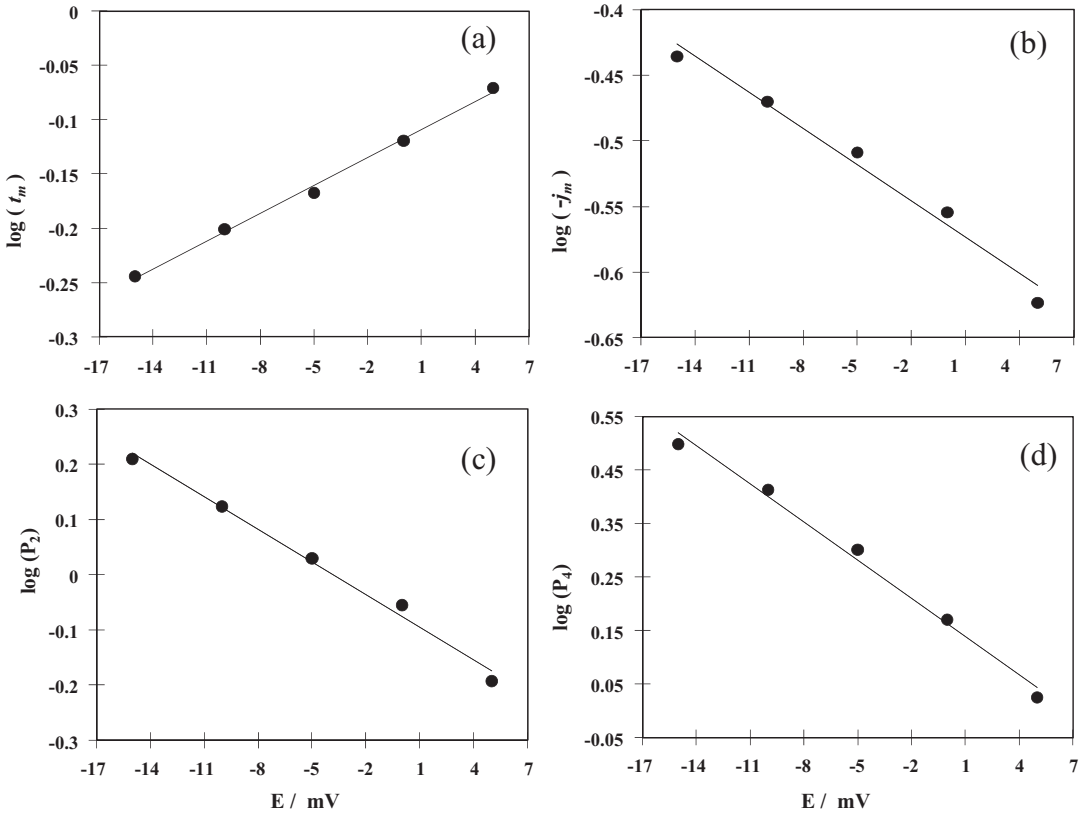

Fig. 12. Potential dependence of (a) $\log t_m$, (b) $\log -j_m$, (c) $\log P_2$ and (d) $\log P_4$. The lines correspond to the data's linear regression.

and the intercept being equal to $\log(K_a^0)$. Fig. 11, shows a plot of the variation of K_2 (see Table 2) as a function of the applied potential. The linear regression analysis shows that the correlation coefficient was 0.98, with a slope $m = 0.0065$ and an intercept of 0.94. Substituting the m value in Eq. (22) it is found that the energy transfer coefficient (β) for this process was 0.99 at 25 °C. Further, from the value of the intercept a value of 8.709 s^{-1} was obtained for K_a^0.

Fig. 12 shows the potential dependence of both the current time's maximas (t_m) and the current's maxima (j_m) of the transients shown in Fig. 9, plus the parameters P_2 (instantaneous nucleation) and P_4 (progressive nucleation). In all cases the observed behavior was linear. The magnitude of the slope was 0.0086 (for the variation of $\log(t_m)$ with E), −0.009 (for the straight line $\log(-j_m)$ vs. E), −0.0197 (for the P_2 variation) and −0.0238 (in the case of P_4).

It should be noted that $(\partial \log -j_m/\partial E) \cong -(\partial \log t_m/\partial E)$ describes the 2D nucleation model, either for the instantaneous or the progressive nucleation [28]. Furthermore, it can be expected that for the case of instantaneous nucleation $(\partial \log t_m/\partial E) \cong -(1/2)(\partial \log P_2/\partial E)$ and for the case of the progressive nucleation $(\partial \log t_m/\partial E) \cong -(1/3)(\partial \log P_4/\partial E)$. The experimental results fulfill these two requisites adequately. Thus, a good support is given to each of the contributions so that the model proposed (refer to Eq. (19)) as well as the results of the fitting method to the experimental data, explain the UPD copper deposit in this system under the conditions stated.

Table 3 shows the values of the charge involved as a function of the potential in each of the processes comprising the transient of Eq. (19). It can be observed that as the potential becomes more cathodic, the charge involved in the 2D progressive nucleation process ($q_{2Dp\text{-}LI}$), decreases while the opposite is true for the charge associated to the 2D instantaneous nucleation process ($q_{2Di\text{-}LI}$). In spite of this, the overall charge due to the nucleation process ($q_{nucleation}$) is practically independent of the applied potential. The same can be said of the charge due to the adsorption process (q_{ad}). It is worthwhile noting that the overall charge ($q_{nucleation} + q_{ad}$) corresponds quite well to that reported for the formation of a monolayer,

Table 3
Variation of the charge involved in each of the processes participating in the formation of a copper monolayer deposited, under UPD conditions on the Au(1 1 1) electrode, as a function of the applied potential.

E/mV	$-q_{2Di\text{-}LI}$/μC cm^{-2} (a)	$-q_{2Dp\text{-}LI}$/μC cm^{-2} (b)	$-q_{nucleation}$/μC cm^{-2} (c)	$-q_{ad}$/μC cm^{-2} (d)	$-q_{total}$/μC cm^{-2} (e)	$\%q_{nucleation}$	$\%q_{adsorption}$
−15	210.5	72.24	282.7	169.0	451.7	62.60	37.40
−10	185.9	90.14	276.1	160.1	436.16	63.30	36.71
−5	162.26	105.77	268.0	157.6	425.7	62.96	37.03
0	156.6	105.91	262.5	157.9	420.5	62.43	37.56
5	146.4	106.74	253.1	147.0	400.16	63.25	36.75

(a) $q_{2Di\text{-}LI} = P_1/2P_2$.
(b) $q_{2Dp\text{-}LI} = P_3/3P_4$.
(c) $q_{nucleation} = q_{2Di\text{-}LI} + q_{2Dp\text{-}LI}$.
(d) $q_{ad} = k_1/k_2$.
(e) $q_{total} = q_{nucleation} + q_{ad}$.

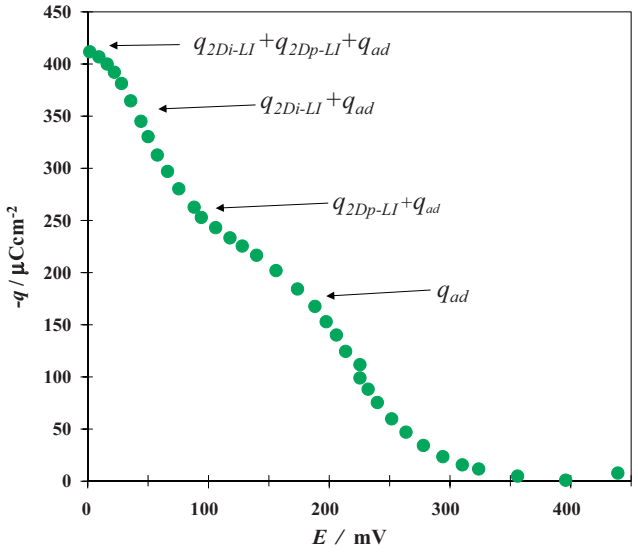

Fig. 13. Charge density variation as a function of the potential, observed during UPD copper deposit on Au(1 1 1) electrode from a 1.0 mM $CuSO_4$, 0.1 M H_2SO_4 aqueous solution at pH 1. The charge density at each potential was estimated through integration of the voltammetric plot (direct scan) shown in Fig. 1. The arrows mark approximately the charge associated to each of the processes participating in the formation of the copper monolayer.

particularly at −10 mV potential; also, it is can be remarked that in all cases the overall process occurred with only 60% of the charge due to nucleation and the remnant 40% was due to adsorption.

Fig. 13 shows the experimental estimate of the charge density variation with the potential, during UPD copper deposition onto Au(1 1 1), carried out through integration of the voltammetric plot (in the cathodic direction) shown in Fig. 1. The arrows mark approximately the transitions observed for theoretical average values that (see Table 3) correspond to various charge densities of the processes involved in the mechanism proposed to explain the transients shown in Fig. 9.

It is important to note that, for instance, the average value of the charge density due to the adsorption process (q_{ad}) corresponds to a potential value related to the first transition of the copper deposit's structure: from random to $\left(\sqrt{3}\times\sqrt{3}\right)$ R30° (see Fig. 2). Also, the value of the sum of the charge density for adsorption and the charge density due to the 2D progressive nucleation process ($q_{2Dp\text{-}LI}$), corresponds to a potential in the second transition zone: from $\left(\sqrt{3}\times\sqrt{3}\right)$ R30° to (1×1). The sum of the charge density of the two processes, that of nucleation and that of adsorption ($q_{ad}+q_{2Dp\text{-}LI}+q_{2Di\text{-}LI}$) corresponds to a potential value related with the structure (1×1). The different contributions comprised in the transient in Eq. (19) could be related to the structural changes observed during the copper underpotential deposition onto Au(1 1 1). The current j_{ad} relates with the random adsorption of copper atoms, the $j_{2Dp\text{-}LI}$ with the ordered honeycombe structure and, lastly, the $j_{2Di\text{-}LI}$ with the (1×1) structure. The use of gold single crystal surfaces to study the copper electrodeposition at UPD, made it possible to associate each of the individual contributions from which the overall current of the experimental potentiostatic current transients has been deconvoluted. It is important to mention that Baré and Buess-Herman [37] have successfully used Hölzle et al., model [3] to describe experimental current transients recorded during the formation of two-dimensional uracil ordered phases at the gold single crystal electrode where three-stage process were involved.

3.3.3. *Electrochemical formation of a copper monolayer onto Au polycrystalline*

From the previous analysis, it becomes clear that regardless of the crystalline nature of the Au electrode during the copper UPD processes taking place, a metal monolayer was formed (see Fig. 3), though based on the apparent large difference of the corresponding transients (see Fig. 4), the formation of the said monolayer should

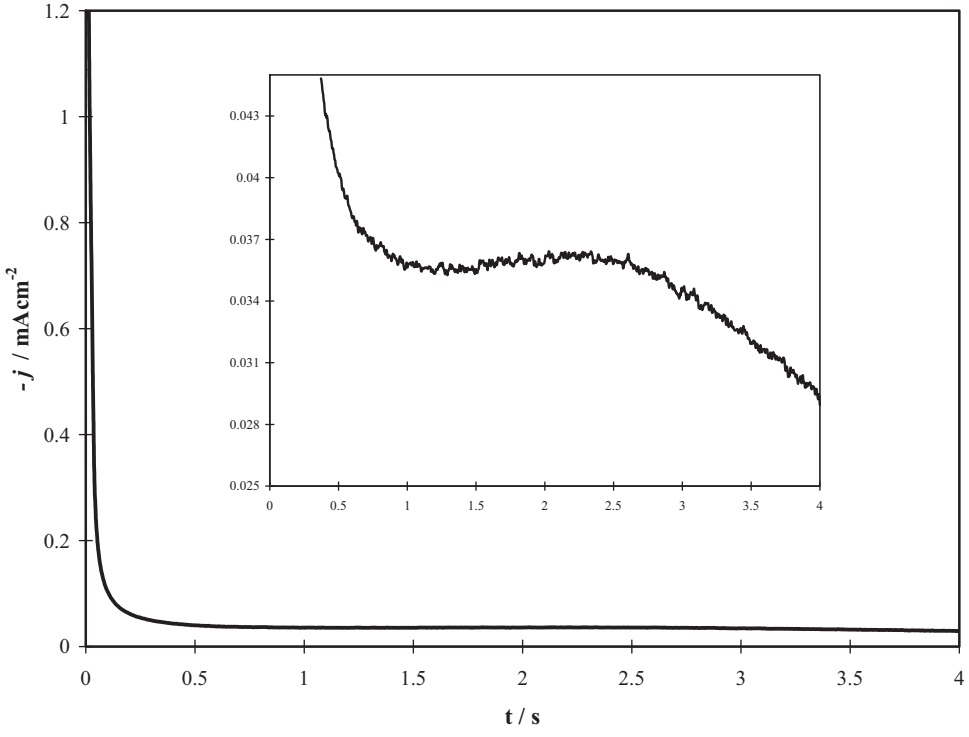

Fig. 14. Potentiostatic current transients obtained during copper underpotential deposition onto polycrystalline gold from a 1.0 mM $CuSO_4$, 0.1 M de H_2SO_4 aqueous solution at pH 1. The potential step started at E_{ar} = 600 mV and ended at 5 mV. The inset shows a zoom of the current in the 0.025–0.045 mA cm^{-2} range.

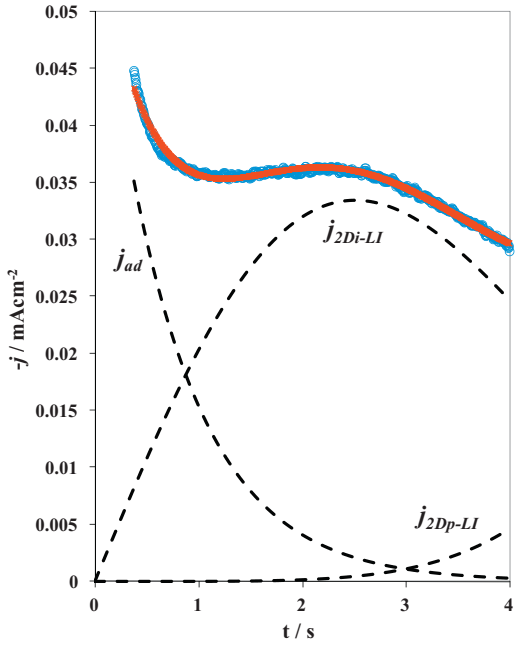

Fig. 15. Comparison between the experimental potentiostatic current transient (blue circles) obtained during formation of a copper monolayer onto polycrystalline gold electrode, under the conditions stated in Fig. 14, and a theoretical transient (red) obtained through non-linear fitting of Eq. (19) to the experimental data. The individual contributions to the overall current have also been plotted that are due to an adsorption process (j_{ad}), a progressive 2D nucleation process limited by ad-atom incorporation ($j_{2Dp\text{-}LI}$) and an instantaneous 2D nucleation process, limited also by incorporation of ad-atoms ($j_{2Di\text{-}LI}$). (For interpretation of the references to color in this figure legend, the reader is referred to the web version of the article.)

involve quite different mechanisms. However, when observing carefully (refer to inset in Fig. 14), the corresponding transient for polycrystalline gold shows that there exists a significant likeness between both transients. From the similitude we propose to use also Eq. (19) to describe the formation process of the copper monolayer onto polycrystalline gold. Fig. 15 shows the comparison between the plot of the experimental potential transient data and the theoretical one generated through non linear fitting of Eq. (19) to the said data; as is customary, the figure also shows the individual contributions to the overall current. Thus, the mechanism proposed does indeed look appropriate to describe the formation process of the copper monolayer onto the polycrystalline gold substrate. However, the kinetics for the process appears different and, for the present case, the nucleation process is mainly due to the 2Di-LI process.

4. Conclusions

The potentiostatic formation of a full copper monolayer onto the gold electrode under UPD conditions follows the same mechanism, regardless of the crystallinity of the substrate (single crystal or polycrystalline). The mechanism involved the simultaneous presence of an adsorption process and of two 2D nucleation processes, progressive and instantaneous, respectively.

The use of gold (1 1 1) surface to study the UPD made it possible to associate each of the individual contributions from which the overall current of the experimental potentiostatic current transient has been deconvoluted.

Acknowledgements

Authors are grateful for financial support from SNI-CONACYT. MPP and MRR like to thank CONACYT for Projects 24658 and 131432. Also MPP, EGG, MRR, MTRS and NB gratefully thank the SNI for the distinction of their membership and the stipend received. EGG, MRR and MPP wish to thank the Departamento de Materiales, UAM-A, for financial support given through Project nos. 2261203, 2261204, 2261205 and 2261208.

References

[1] A. Milchev, Electrocrystallization: Fundamentals of Nucleation and Growth, Kluwer Academic Publishers, The Netherlands, 2002 (Chapter 5).
[2] D.M. Kolb, Schering Lecture's Publication, vol. 2, issue no. 1, Schering Research Foundation, Berlin, 1991.
[3] M.H. Hölzle, U. Retter, D.M. Kolb, J. Electroanal. Chem. 371 (1994) 101.
[4] R.C. Salavarezza, D.V. Vásquez Moll, M.C. Giordano, A.J. Arvia, J. Electroanal. Chem. 213 (1986) 301.
[5] J. Tang, M. Petri, L.A. Kibler, D.M. Kolb, Electrochim. Acta 51 (2005) 125.
[6] H. Hagenstrom, M.A. Schneeweiss, D.M. Kolb, Electrochim. Acta 45 (1999) 1141.
[7] H.-F. Waibel, M. Kleinert, L.A. Kibler, D.M. Kolb, Electrochim. Acta 47 (2002) 1461.
[8] M. Kleinert, H.-F. Waibel, G.E. Engelmann, H. Martin, D.M. Kolb, Electrochim. Acta 46 (2001) 3129.
[9] M.H. Hölzle, V. Zwing, D.M. Kolb, Electrochim. Acta 40 (1995) 1237.
[10] L.H. Mendoza-Huizar, J. Robles, M. Palomar-Pardave, J. Electrochem. Soc. 152 (2005) C265.
[11] X. Zeng, S. Bruckenstein, J. Electrochem. Soc. 146 (1999) 2549.
[12] M.J. Henderson, E. Bitziou, A. Hillman, E. Vieil, J. Electrochem. Soc. 148 (2001) E105.
[13] J.-J. Lee, I.T. Bae, D.A. Scherson, B. Miller, K.A. Wheeler, J. Electrochem. Soc. 147 (2000) 562.
[14] S. Langerock, L. Heerman, J. Electrochem. Soc. 151 (2004) C155.
[15] M. Willis, R. Alkire, J. Electrochem. Soc. 156 (2009) D377.
[16] R. Greef, R. Peat, L.M. Peter, D. Pletcher, J. Robinson, Instrumental Methods in Electrochemistry, Ellis Horwood, Chichester, 1985 (Chapter 9).
[17] B.R. Scharifker, G. Hills, Electrochim. Acta 28 (1983) 879.
[18] B.R. Scharifker, J. Mostany, M. Palomar-Pardavé, I. González, J. Electrochem. Soc. 146 (1999) 1005.
[19] M. Sluyters-Rehbach, J.H.O.J. Wijenberg, E. Bosco, J.H. Sluyters, J. Electroanal. Chem. 283 (1990) 35.
[20] L. Heerman, A. Tarallo, Electrochem. Commun. 2 (2000) 85.
[21] M.Y. Abyaneh, M. Fleischmann, J. Electrochem. Soc. 138 (1991) 2491.
[22] M.H. Hölzle, C.W. Apsel, T. Will, D.M. Kolb, J. Electrochem. Soc. 142 (1995) 3741.
[23] M. Palomar-Pardavé, N. Batina, I. González, J. Phys. Chem. B 104 (2000) 3545.
[24] A. Martínez-Ruíz, M. Palomar-Pardavé, J. Valenzuela-Benavides, M.H. Farias, N. Batina, J. Phys. Chem. B 107 (2003) 11660.
[25] M. Palomar-Pardavé, M. Miranda-Hernández, I. González, N. Batina, Surf. Sci. 399 (1998) 80.
[26] L.H. Mendoza-Huizar, J. Robles, M. Palomar-Pardavé, J. Electroanal. Chem. 521 (2002) 95.
[27] M.R. Majidi, K. Asadpour-Zeynali, B. Hafezi, Electrochim. Acta 54 (2009) 1119.
[28] A. Bewick, M. Fleischmann, H.R. Thirsk, Trans. Faraday Soc. 58 (1962) 2200.
[29] A. Milchev, T. Zapryanova, Electrochim. Acta 51 (2006) 2926.
[30] A. Milchev, T. Zapryanova, Electrochim. Acta 51 (2006) 4916.
[31] M. Palomar-Pardavé, B.R. Scharifker, E.M. Arce, M. Romero-Romo, Electrochim. Acta 50 (2005) 4736.
[32] M.G. Montes de Oca, J. Mostany, M.T. Ramírez-Silva, M. Romero-Romo, B.R. Scharifker, M. Palomar-Pardavé, ECS Trans. 3 (2007) 25.
[33] J. Zhang, Y.-E. Sung, P.A. Rikvold, A. Wieckowski, J. Chem. Phys. 104 (1996) 5699.
[34] P.A. Rikvold, J. Zhang, Y.-E. Sung, A. Wieckowski, Electrochim. Acta 41 (1996) 2175.
[35] G. Brown, P.A. Rikvold, M.A. Novotny, A. Wieckowski, J. Electrochem. Soc. 146 (1999) 1035.
[36] M. Noël, K. Vasu, Cyclic Voltammetry and the Frontiers of Electrochemistry Aspect, London, 1990 (Chapter 7).
[37] S. Baré, C. Buess-Herman, Colloids Surf. A 134 (1998) 181.